NASA TN D-728

NASA TN D-728

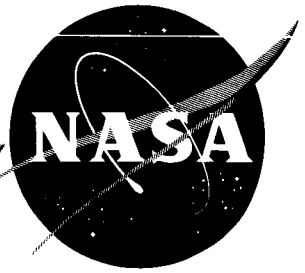

TECHNICAL NOTE

D-728

EXPERIMENTAL INVESTIGATION OF A HIGH-SPEED HYDROFOIL WITH PARABOLIC THICKNESS DISTRIBUTION AND AN ASPECT RATIO OF 3

By Kenneth W. Christopher

Langley Research Center
Langley Field, Va.

NATIONAL AERONAUTICS AND SPACE ADMINISTRATION

WASHINGTON

March 1961

NATIONAL AERONAUTICS AND SPACE ADMINISTRATION

TECHNICAL NOTE D-728

EXPERIMENTAL INVESTIGATION OF A HIGH-SPEED HYDROFOIL WITH PARABOLIC THICKNESS DISTRIBUTION AND AN ASPECT RATIO OF 3

By Kenneth W. Christopher

SUMMARY

An experimental investigation has been made to determine the hydrodynamic characteristics of a 10-percent-thick hydrofoil with an aspect ratio of 3 designed to operate with acceptable efficiency at speeds in the neighborhood of 100 knots (169 fps). A cambered hydrofoil model with a parabolic thickness distribution was investigated at a depth of 1/2 chord over a range of angles of attack from -0.5° to 4.0° and at speeds from 120 to 210 fps. The hydrofoil of this investigation had a substantially wider range of operation at acceptable lift-drag ratios as well as higher maximum lift-drag-ratio values than did a hydrofoil of similar design with an aspect ratio of 1.

INTRODUCTION

A hydrofoil designed for efficient operation at speeds in the neighborhood of 100 knots will usually be very thin. A hydrofoil designed to operate fully wetted using conventional airfoil shapes must be thin to avoid cavitation on its upper surface, and a supercavitating hydrofoil must be thin particularly near the sharp leading edge to avoid wetting of its upper surface. Thin sections, however, cause considerable structural problems.

A relatively thick hydrofoil that would operate with acceptable efficiency at speeds in the neighborhood of 100 knots would be desirable for structural reasons. Design principles for such a hydrofoil are given in reference 1 along with the results of an experimental investigation of an aspect-ratio-1 hydrofoil so derived. This hydrofoil had a parabolic thickness distribution and a thickness ratio of 0.10.

The parabolic leading edge and higher thickness ratio of the parabolic section makes higher aspect ratios structurally feasible for practical applications. Therefore, a hydrofoil with a rectangular planform

and an aspect ratio of 3 was derived and its characteristics were briefly determined in the Langley high-speed hydrodynamics facility. The results of this investigation are reported herein.

SYMBOLS

A	aspect ratio
a	mean-line designation, fraction of chord from leading edge over which design load is uniform
C_L	lift coefficient, $\frac{\text{Lift}}{qS}$
C_D	drag coefficient, $\frac{\text{Drag}}{qS}$
C_{cp}	center-of-pressure coefficient, $\frac{\text{Distance from leading edge to center of pressure}}{\text{Chord}}$
$C_{L,d}$	three-dimensional design lift coefficient
$c_{l,d}$	two-dimensional design lift coefficient
d/c	depth of submersion with respect to chord, measured from local mean water surface to leading edge of hydrofoil
E	ratio of planform semiperimeter to span
L/D	lift-drag ratio
$p_{c,b/2}$	cavity pressure measured at hydrofoil midspan, lb/sq ft
$p_{c,t}$	cavity pressure measured near tip of hydrofoil, lb/sq ft
p_o	free-stream pressure at local mean depth of hydrofoil, lb/sq ft
q	free-stream dynamic pressure, lb/sq ft
S	hydrofoil area, sq ft

V	speed, fps and knots
X,Y	coordinate axes, with origin at leading edge of hydrofoil
x	distance from leading edge of hydrofoil along X-axis, in.
x_s	distance from leading edge of strut along center line, in.
y_s	perpendicular distance from center line to strut surface, in.
y_l	perpendicular distance from X-axis to lower surface of hydrofoil, in.
y_u	perpendicular distance from X-axis to upper surface of hydrofoil, in.
α	hydrofoil angle of attack, measured from X-axis of section, radians unless otherwise specified
α_i	induced angle of attack, radians unless otherwise specified
$\sigma_{b/2}$	cavitation number based on cavity pressure measured at hydrofoil midspan, $\frac{p_o - p_{c,b/2}}{q}$
σ_t	cavitation number based on cavity pressure measured near tip of hydrofoil, $\frac{p_o - p_{c,t}}{q}$
τ	planform correction factor

DESCRIPTION OF MODEL

A sketch and the coordinates of the hydrofoil model are given in figure 1. Photographs of the hydrofoil are presented in figure 2. The hydrofoil had a span of 12.250 inches, a chord of 4.083 inches, a planform area of 50 square inches, and a ratio of base thickness to chord of 0.1.

The hydrofoil had a parabolic thickness distribution with the vertex at the nose and was designed to have a three-dimensional lift coefficient of 0.14 for comparison with the hydrofoil with an aspect ratio of 1 (ref. 1). The amount of camber necessary to achieve this design

lift coefficient was determined in the same manner as in reference 1 - that is, by stating that the design lift coefficient is that realized when $\alpha = \alpha_i$ in the following equation:

$$C_L = \frac{1}{E}\left[c_{l,d} + 2\pi(\alpha - \alpha_i)\right]$$

where

C_L lift coefficient at finite aspect ratio

E ratio of planform semiperimeter to span and is $\frac{A + 1}{A}$ for rectangular planforms where A is aspect ratio

$c_{l,d}$ two-dimensional lift coefficient produced by camber of section

α geometrical angle of attack defined as $\alpha = 0$ when total two-dimensional lift coefficient is $c_{l,d}$

α_i induced angle of attack, $(1 + \tau)\frac{C_L}{\pi A}$ where τ is correction for planform (ref. 2)

Then

$$C_{L,d} = \frac{A}{A + 1} c_{l,d}$$

which gives, for $C_{L,d} = 0.14$ and $A = 3$, a value for $c_{l,d}$ of 0.1867. An a = 1.0 mean line (ref. 3) was then used that would produce a two-dimensional design lift coefficient of 0.1867.

The model was supported by a parabolic strut (fig. 1) having a 4.0-inch chord and a ratio of base thickness to chord of 0.15.

APPARATUS AND PROCEDURE

Facility

The model was tested in the Langley high-speed hydrodynamics facility which is described in reference 4; however, a different carriage was used (ref. 1). A photograph of this carriage is shown in figure 3. The high-speed carriage is operated in the same manner as the one described in reference 4.

Balance

Lift, drag, and pitching moment were measured by an electrical strain-gage balance attached to a hydraulically operated towing staff located on the end of the boom overhanging the tank (fig. 3). The forces were continuously recorded on strip-chart recorders located in the instrument house. Force measurements were read at three photographic stations at which water-level readings were available. Speeds were measured at each station by electrically measuring the time for the carriage to travel a distance of 10 feet. A magnetic device was employed to indicate on the records when the carriage passed a photographic station.

The angle of attack was measured from the horizontal to the X-axis of the hydrofoil section shown in figure 1. Changes in angle of attack due to structural deflections were obtained during the calibration of the balance, and all angles of attack were increased by 4 minutes to allow for deflections caused by the loads expected in these tests.

Pressures

Pressures in the cavity aft of the hydrofoil were measured at two positions on the center of the base of the hydrofoil. One pressure orifice was located at the midspan position and the other was 1 inch inboard from the tip (fig. 2). These pressures were continuously recorded by an oscillograph located in the instrument house.

Photographs

Photographs of the flow about the model were taken from above water at the three stations at which force readings were obtained. Underwater photographs were also taken through a window in the bottom of the tank.

Scope

The depth of submersion of the leading edge of the hydrofoil was set at 2.0 inches (1/2 chord) at the start of each test and any variations from this setting were recorded. The hydrofoil was investigated at angles of attack between -0.5° and 4.0° and at speeds from 120 to 210 fps. The density of the tank water used in computing the force coefficients was 1.94 slugs/cu ft. The kinematic viscosity during the test was 1.58×10^{-5} sq ft/sec.

RESULTS AND DISCUSSION

The experimental data obtained in this investigation are presented in table I. The variations of force coefficients, center-of-pressure coefficient, and lift-drag ratio with speed are shown in figures 4 to 7.

As shown in figure 4, lift coefficient decreased with increase in speed for angles of attack from 0° to 2.0°. This decrease in lift coefficient was caused by the increase in cavitation on and ventilation of the upper surface of the hydrofoil with increase in speed. For angles of attack greater than 2.0° the flow separated from the upper surface of the hydrofoil at all speeds and the lift coefficient became independent of speed. Although at an angle of attack of -0.5° the upper surface of the hydrofoil was fully wetted at all speeds, cavitation was photographically observed to occur on the bottom of the hydrofoil at the leading edge and this bottom-surface cavitation is the probable reason for the slight decrease in lift coefficient with increase in speed at this angle of attack.

Drag coefficient shown in figure 5 was that obtained after removing the calculated form, friction, and base-pressure drag of the strut but not the base-pressure drag of the hydrofoil.

Values of lift-drag ratio (fig. 6) show a general decrease with increase in speed similar to the lift-coefficient variation. The curves in figure 6 are based on the faired values of figures 4 and 5.

The variation of center-of-pressure coefficient with speed is shown in figure 7. When the upper surface of the hydrofoil was wetted or partly wetted, the center of pressure moved forward with increase in speed. For the angle of attack of -0.5°, the center of pressure moved aft with increase in speed as would be expected with increasing cavitation on the lower surface at the leading edge. At an angle of attack of 4.0°, the flow is separated from the upper surface of the hydrofoil and the center-of-pressure position does not vary with speed.

Photographs of the flow about the hydrofoil for three angles of attack are shown in figure 8. The upper surface of the hydrofoil was fully wetted at an angle of attack of 0°. At an angle of attack of 1.5°, several patches of cavitation may be seen, the one at the mid-semispan and the tip vortex being vented to the atmosphere through the cavity aft of the hydrofoil and strut. The upper surface of the hydrofoil is almost fully vented at an angle of attack of 3.0° with small areas of attached flow near the leading edge between the cavity streaks that are vented through the wake of the hydrofoil. (Cavitation originated from discrete points on the leading edge of the hydrofoil although no surface irregularities were noticeable on the hydrofoil.)

A crossplot showing the lift and drag coefficients against angle of attack at constant speeds of 80, 90, and 100 knots (135, 152, and 169 fps) is shown in figure 9(a). The data points correspond to the fairings from figures 4 and 5. As can be seen, the lift-curve slope decreased with increase in speed. At 80 knots, a fairly abrupt decrease in lift coefficient is indicated between the angles of attack of 2.0° and 3.0° as the amount of flow separation from the top surface increased rapidly with increase in angle of attack. At higher speeds, flow separation occurred more gradually with increase in angle of attack and started at lower angles of attack so that at these higher speeds less lift than that for 80 knots was realized at angles of attack less than 3.0°.

The variation of drag coefficient with angle of attack shows a marked decrease in drag coefficient at angles of attack of 0° and 0.5° for speeds of 80 and 90 knots. This local variation appears similar to the drag "bucket" obtained with some airfoils designed for laminar flow and seems reasonable in view of the favorable gradients existing on the parabolic thickness distribution. Since at 100 knots this "bucket" was not realized, it probably would not occur on a full-scale hydrofoil which would operate at a higher Reynolds number.

Lift-drag ratio plotted against angle of attack is shown in figures 9(b) and 9(c). The solid curves of figure 9(b) were obtained from the faired values of lift and drag coefficients of figure 9(a). As can be seen, a maximum value of 12.4 is obtained at an angle of attack of 0.5°. The dashed curves of figure 9(b) were obtained from figure 9(a) by discounting the drag "bucket" which may not exist for a full-scale hydrofoil. These curves indicate a maximum lift-drag ratio of about 10.6. It may be noted that the maximum lift-drag ratio occurs between angles of attack of 0.5° and 1.0° for the fully wetted condition (80 knots). This result is in fair agreement with the three-dimensional design angle of attack which is roughly $\frac{0.14}{\pi A}$ or 0.85° (the effect of the proximity of the water surface, which would increase this value somewhat, being neglected).

An inspection of the recorded cavity pressures indicated that the wake of the hydrofoil and strut was not fully ventilated to the atmosphere. An improvement in lift-drag ratio could be expected if the base of the hydrofoil were fully ventilated. In figure 9(c) (solid curves) are shown the values of lift-drag ratios obtained when the base drag of the hydrofoil is removed from the experimental data. An average value for base-drag coefficient was determined from the measured base pressures for each angle of attack and was subtracted from the faired drag-coefficient values of figure 9(a) (the "bucket" being discounted). As shown in figure 9(c) a maximum value of lift-drag ratio of about 14.3 is indicated for the fully ventilated condition.

The variation of lift-drag ratio with lift coefficient is shown in figure 10. The curves shown in figure 10(a) are the same as the dashed curves of figures 9(b) and 9(c). The lift-drag ratios of the model without hydrofoil base drag are shown plotted against lift coefficient in figure 10(b).

A comparison of the lift-drag ratios of the present investigation with those of the hydrofoil of similar design with an aspect ratio of 1 (ref. 1) is shown in figure 11. The lift-drag ratios of figure 10(a) are shown (hydrofoil base drag not removed) for direct comparison with the hydrofoil data of reference 1. An appreciable increase in lift-drag ratio as well as a broadening of the range of lift coefficient for high lift-drag-ratio values with an increase in aspect ratio is indicated.

CONCLUDING REMARKS

A brief investigation has been conducted to determine the hydrodynamic characteristics of a 10-percent-thick hydrofoil with an aspect ratio of 3, designed to operate with acceptable efficiency near speeds of 100 knots, and to compare the performance of this hydrofoil with a hydrofoil of similar design with an aspect ratio of 1. The cambered hydrofoil having a parabolic thickness distribution and an aspect ratio of 3 had, as would be expected, characteristics similar to the hydrofoil with a similar cross section and an aspect ratio of 1. These characteristics were: a narrow range of angle of attack for optimum efficiency, and force changes caused by transition from a wetted to a vented upper surface with increase in angle of attack or speed. The cambered parabolic hydrofoil with an aspect ratio of 3 had a substantially wider range of operation at acceptable lift-drag ratios as well as higher maximum lift-drag-ratio values than did the cambered parabolic hydrofoil with an aspect ratio of 1.

Langley Research Center,
National Aeronautics and Space Administration,
Langley Field, Va., December 27, 1960.

REFERENCES

1. Johnson, Virgil E., Jr., and Rasnick, Thomas A.: Investigation of a High-Speed Hydrofoil With Parabolic Thickness Distribution. NASA TN D-119, 1959.

2. Glauert, H.: The Elements of Aerofoil and Airscrew Theory. Second ed., Cambridge Univ. Press, 1947. (Reprinted 1948.)

3. Abbott, Ira H., Von Doenhoff, Albert E., and Stivers, Louis S., Jr.: Summary of Airfoil Data. NACA Rep. 824, 1945. (Formerly NACA WR L-560.)

4. Christopher, Kenneth W.: Investigation of the Planing Lift of a Flat Plate at Speeds up to 170 Feet Per Second. NACA TN 3951, 1957.

TABLE I.- TEST DATA

α, deg	V, fps	d/c	C_L	C_D	C_{cp}	$\sigma_{b/2}$	σ_t
4.0	141.75	0.60	0.1476	0.0222	0.091	0.0144	0.0125
	134.35	.59	.1460	.0223	.088	.0125	.0108
	128.16	.69	.1463	.0230	.071	.0137	.0119
	188.53	.51	.1496	.0234	.080	.0050	.0037
	177.41	.56	.1467	.0236	.078	.0057	.0041
	169.17	.64	.1431	.0227	.080	.0063	.0045
	168.07	.52	.1476	.0216	.105	.0109	.0090
	159.63	.57	.1462	.0233	.078	.0085	.0085
	152.96	.53	.1447	.0230	.073	.0088	.0084
3.0	141.03	0.63	0.1269	0.0181	0.098	0.0129	0.0132
	130.51	.62	.1275	.0180	.085	.0122	.0125
	121.20	.60	.1326	.0184	.088	.0158	.0132
	168.56	.48	.1255	.0186	.121	.0085	.0101
	156.87	.47	.1254	.0188	.104	.0069	.0086
	147.12	.44	.1243	.0184	.093	.0078	.0089
	185.44	.63	.1261	.0185	.109	.0181	.0175
	172.27	.67	.1252	.0179	.133	.0188	.0183
	161.85	.64	.1233	.0180	.117	.0170	.0158
2.0	146.77	0.59	0.1247	0.0154	0.179	0.0335	0.0342
	135.89	.62	.1295	.0151	.209	.0371	.0375
	126.58	.61	.1493	.0158	.212	.0385	.0410
	175.81	.61	.1100	.0152	.139	.0219	.0237
	162.78	.62	.1143	.0156	.146	.0256	.0263
	152.18	.61	.1195	.0157	.156	.0328	.0313
	190.84	.55	.1060	.0150	-----	.0202	.0188
	177.21	.58	.1081	.0123	.292	.0214	.0200
	166.28	.57	.1077	.0138	.255	.0230	.0217
1.5	159.01	0.57	0.1077	0.0136	0.193	0.0335	0.0336
	147.00	.59	.1182	.0142	.179	.0348	.0354
	136.63	.56	.1268	.0143	.209	.0372	.0380
	165.30	.55	.1067	------	-----	.0308	.0300
	154.11	.56	.1125	.0145	.180	.0334	.0329
	144.75	.58	.1171	.0142	.193	.0344	.0345
	183.47	.58	.0994	.0133	.162	.0265	.0271
	171.23	.61	.1051	.0113	.250	.0269	.0293
	161.26	.60	.1062	.0126	.194	.0299	.0312

TABLE I.- TEST DATA - Concluded

α, deg	V, fps	d/c	C_L	C_D	C_{cp}	$\sigma_{b/2}$	σ_t
1.0	198.70	0.57	0.0891	0.0128	0.146	0.0259	0.0280
	183.50	----	.0940	.0124	.172	.0277	.0306
	171.48	.59	.0973	.0127	.205	.0339	.0316
	149.71	.56	.1111	.0124	.212	.0301	.0302
	140.19	.56	.1237	.0126	.236	.0332	.0340
	131.99	.59	.1423	------	-----	.0333	.0323
	174.76	.52	.0950	.0127	.149	.0295	.0314
	163.02	.58	.1012	.0126	.180	.0321	.0339
	154.02	.50	.1072	.0123	.192	.0303	.0306
0.5	151.61	0.52	0.1154	0.0124	0.383	0.0243	0.0269
	139.93	.52	.1208	------	-----	------	------
	130.00	.52	.1303	------	-----	------	------
	170.11	.56	.0943	------	-----	------	------
	156.68	----	.1116	------	-----	------	------
	146.31	.54	.1161	------	-----	------	------
	185.66	.57	.0831	.0114	.232	.0248	.0281
	171.86	----	.0958	.0113	.252	.0268	.0295
	160.44	.55	.1071	.0117	.274	.0308	.0331
	146.93	.56	.1112	.0106	.350	.0282	.0254
	138.46	.57	.1196	.0097	.345	.0304	.0281
	130.68	.55	.1199	.0097	.348	.0312	.0294
	178.39	.51	.0848	.0108	-----	.0295	.0295
	167.58	.57	.0924	.0110	.285	.0303	.0304
	158.28	.61	.1023	.0109	.327	.0324	.0296
	145.90	----	.1205	.0102	.351	.0280	.0280
	136.82	----	.1215	.0106	.331	.0312	.0313
	129.46	----	.1250	.0091	.334	.0296	.0309
0	207.74	0.59	0.0595	------	-----	0.0241	0.0261
	194.20	.60	.0652	0.0114	0.312	.0262	.0276
	184.61	.64	.0647	.0114	.311	.0261	.0293
	179.97	.61	.0695	.0108	.316	.0283	.0303
	169.50	.59	.0744	.0106	.316	.0284	.0292
	158.80	.61	.0806	.0103	.310	.0284	.0294
	164.32	----	.0820	------	-----	.0284	.0310
	154.47	----	.0863	.0104	.341	.0285	.0302
	145.88	----	.0896	.0100	.327	.0291	.0311
	133.32	----	.1059	.0090	.385	.0283	.0287
	125.46	----	.1040	.0091	.343	.0276	.0289
	118.85	----	.1014	.0081	.376	.0273	.0302
-0.5	154.89	0.58	0.0656	0.0095	0.438	0.0251	0.0261
	145.20	.55	.0666	.0102	.402	.0286	.0297
	137.32	.62	.0659	.0095	.398	.0280	.0290
	177.56	.55	.0576	.0098	.475	------	.0264
	165.88	.59	.0615	.0098	.441	------	.0274
	156.89	.65	.0600	.0091	.452	------	.0274

Hydrofoil Coordinates		
x	y_u	y_l
0.000	0.000	0.000
.020	.017	.012
.031	.021	.015
.051	.028	.019
.102	.040	.026
.204	.058	.034
.306	.072	.040
.408	.084	.045
.612	.105	.054
.817	.121	.060
1.021	.136	.067
1.225	.149	.075
1.429	.160	.082
1.633	.170	.089
1.837	.179	.095
2.042	.186	.102
2.246	.193	.110
2.450	.199	.117
2.654	.204	.126
2.858	.208	.134
3.062	.211	.143
3.266	.213	.153
3.471	.214	.162
3.675	.213	.174
3.879	.211	.188
4.083	.204	.206

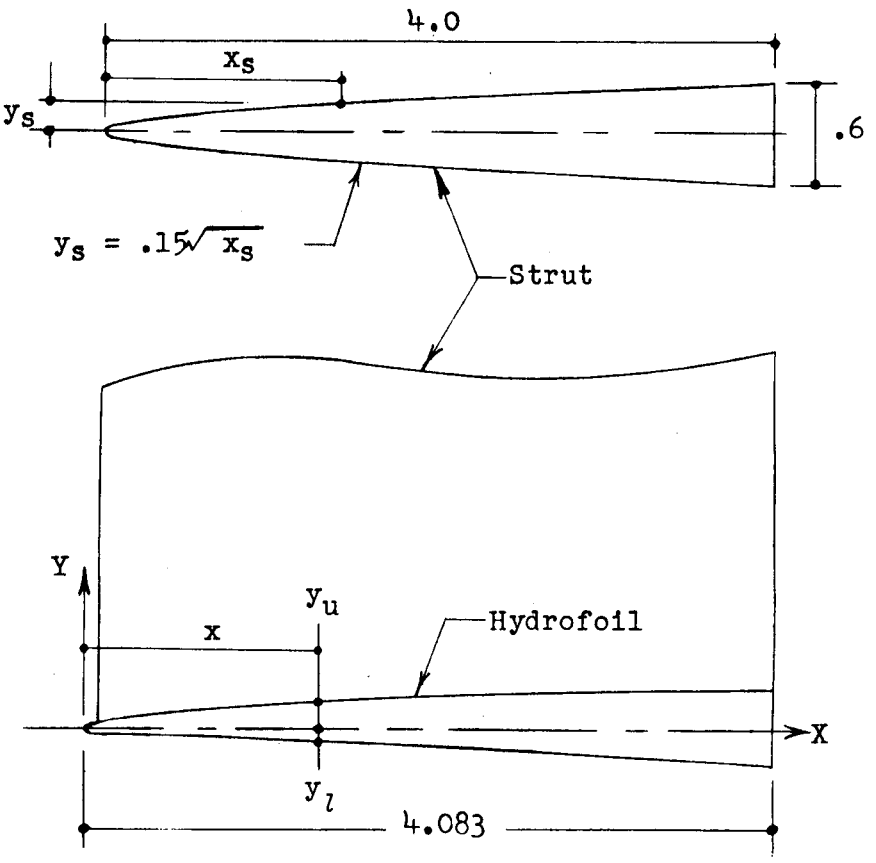

Span = 12.250

Figure 1.- Details of cambered parabolic hydrofoil on strut. All dimensions are in inches.

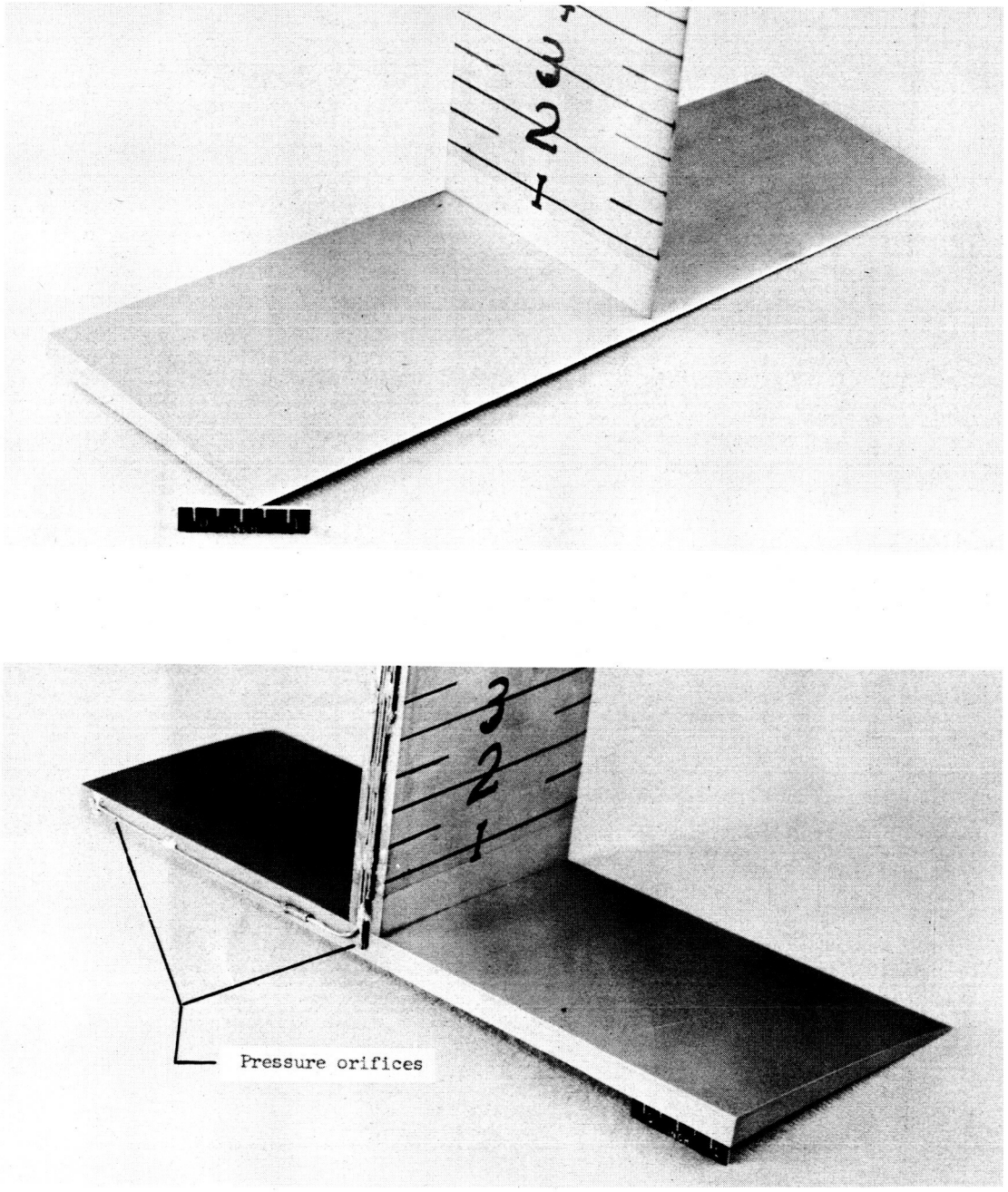

L-60-8324

Figure 2.- Photographs of cambered parabolic hydrofoil with an aspect ratio of 3.

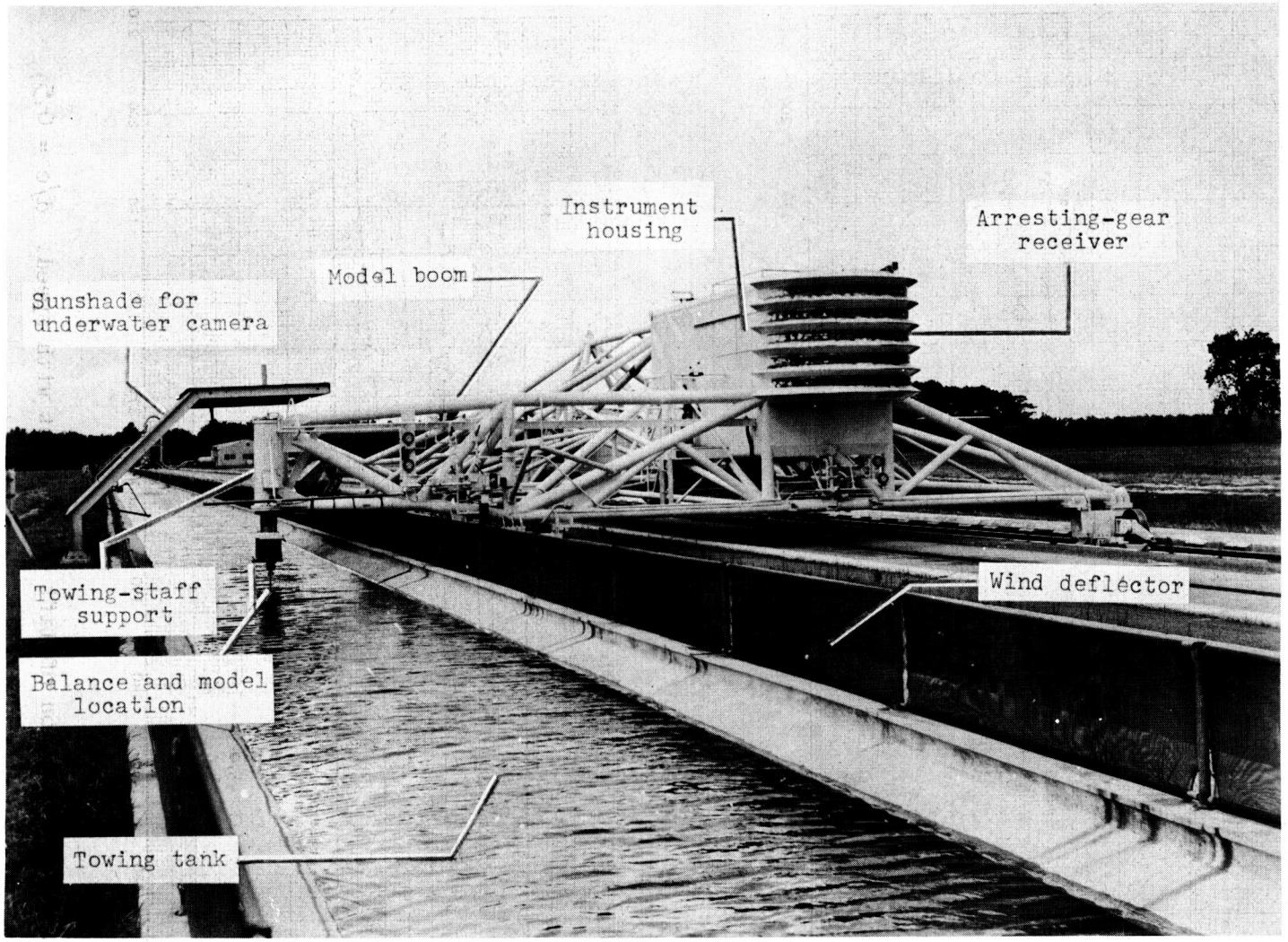

Figure 3.- Photograph of high-speed carriage. L-59-3840.1

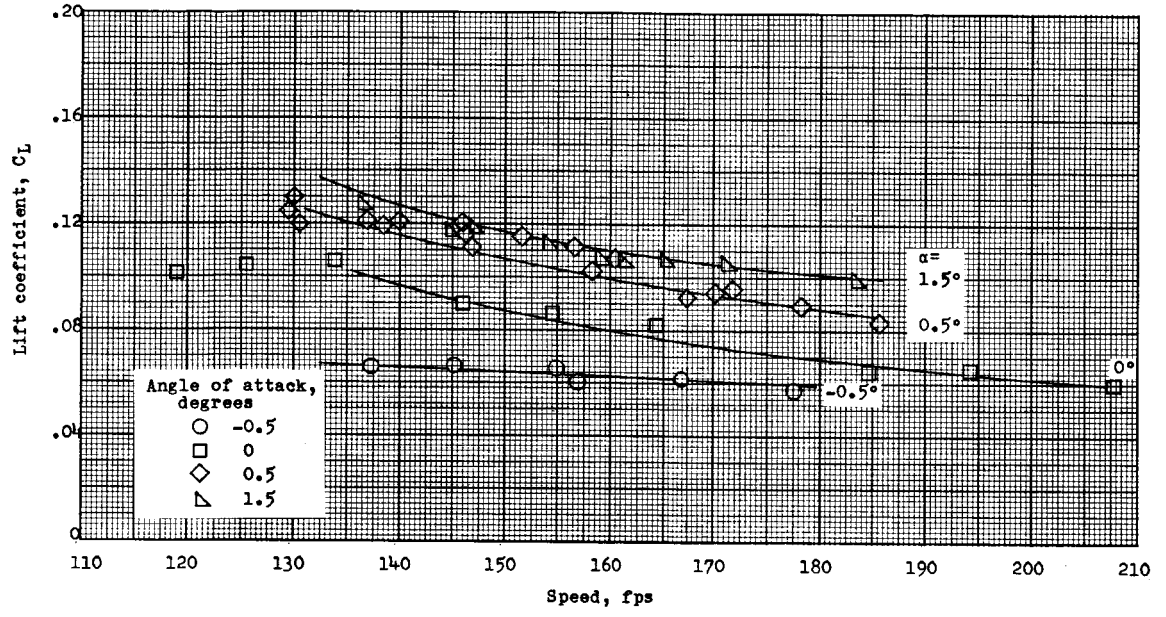

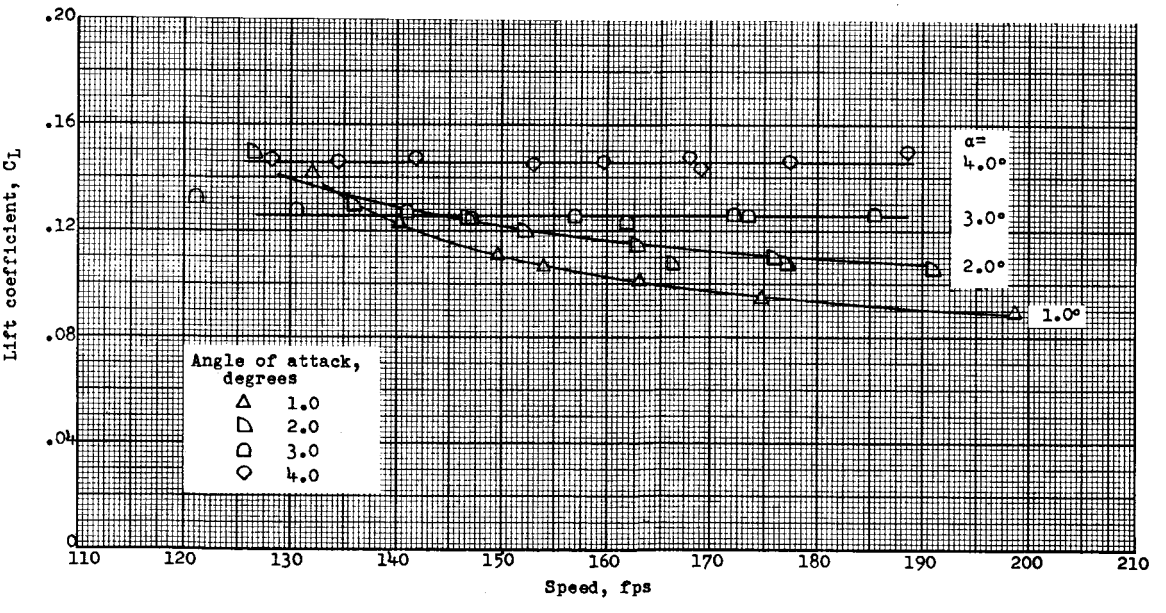

Figure 4.- Variation of lift coefficient with speed. d/c = 0.5.

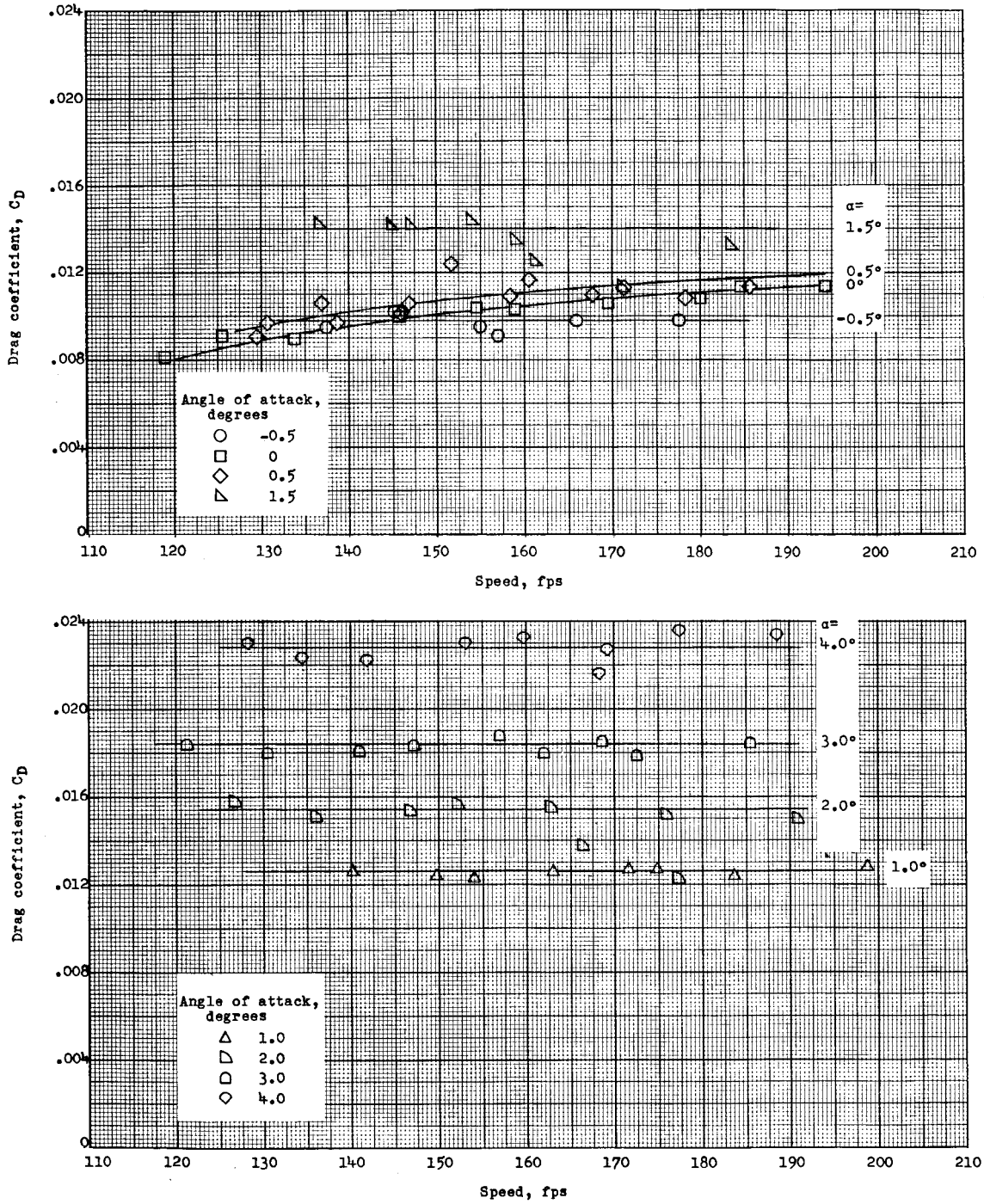

Figure 5.- Variation of drag coefficient with speed. d/c = 0.5.

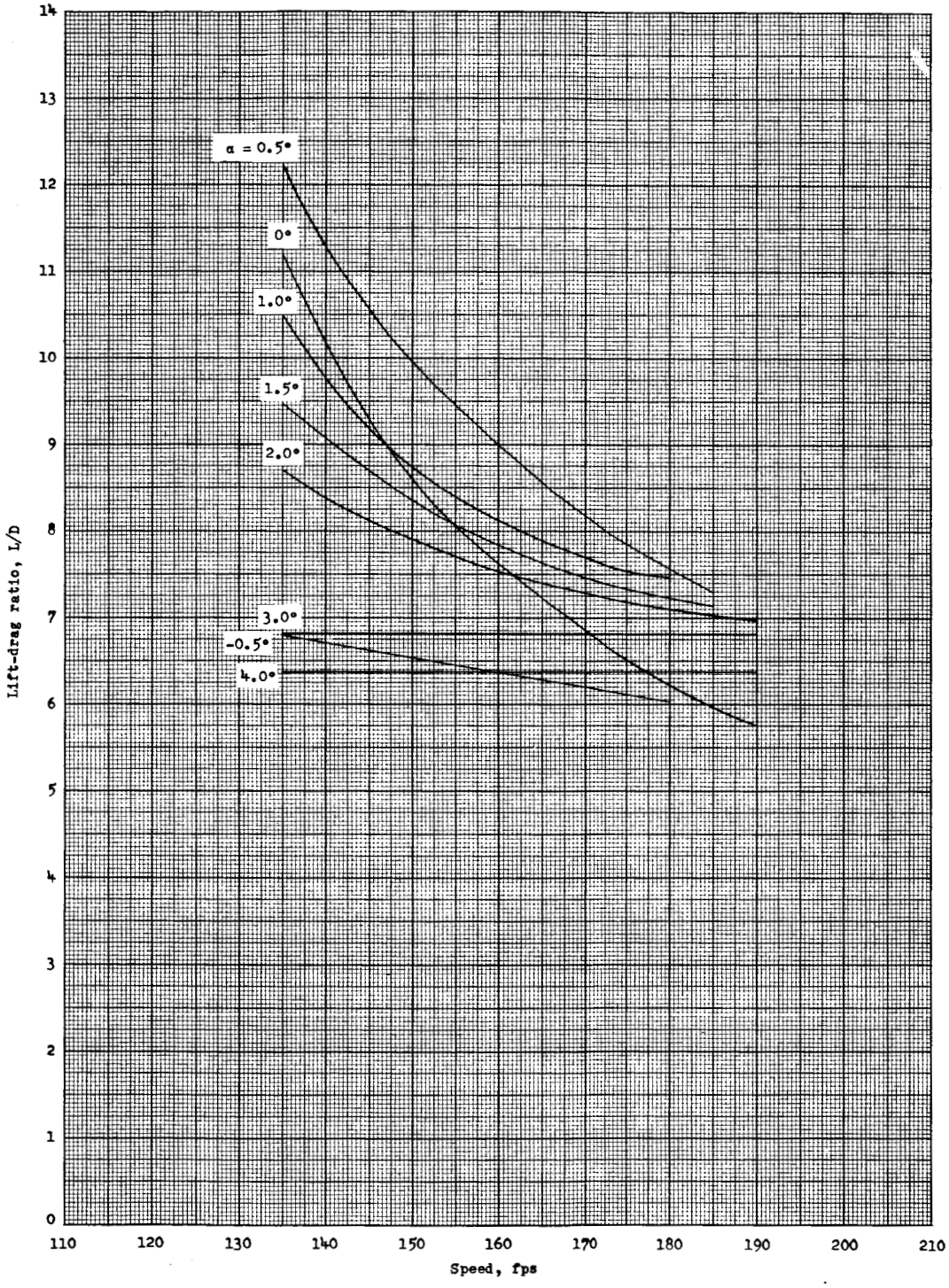

Figure 6.- Variation of lift-drag ratio with speed. d/c = 0.5.

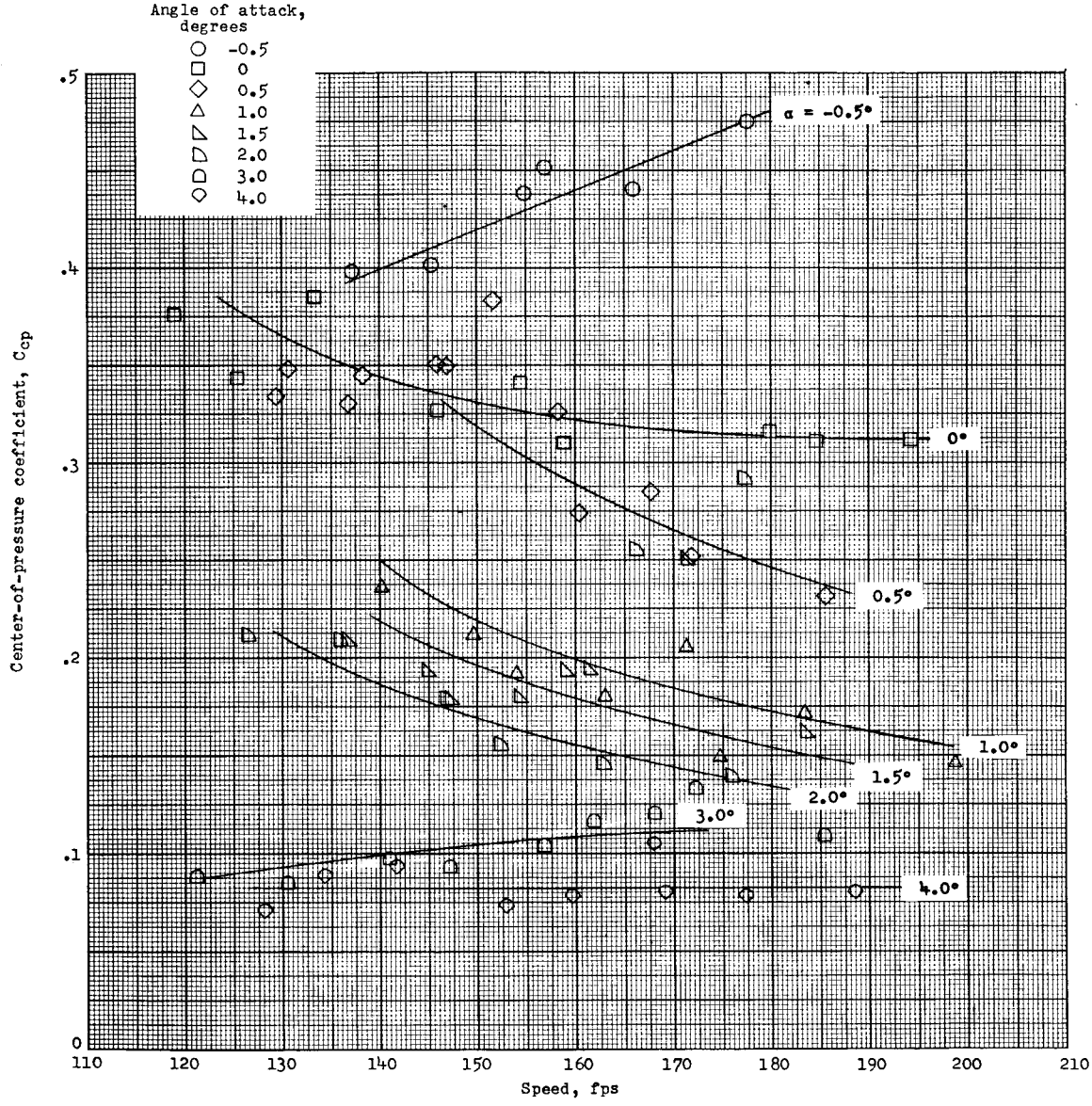

Figure 7.- Variation of center-of-pressure coefficient with speed. d/c = 0.5.

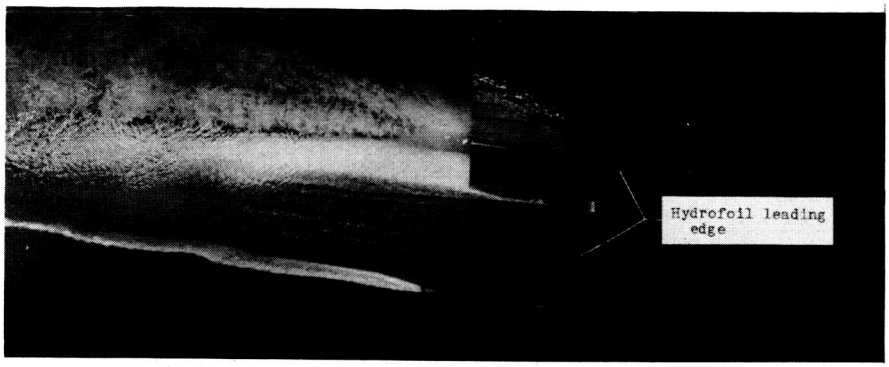

(a) $\alpha = 0^{\circ}$; V = 145.88 fps.

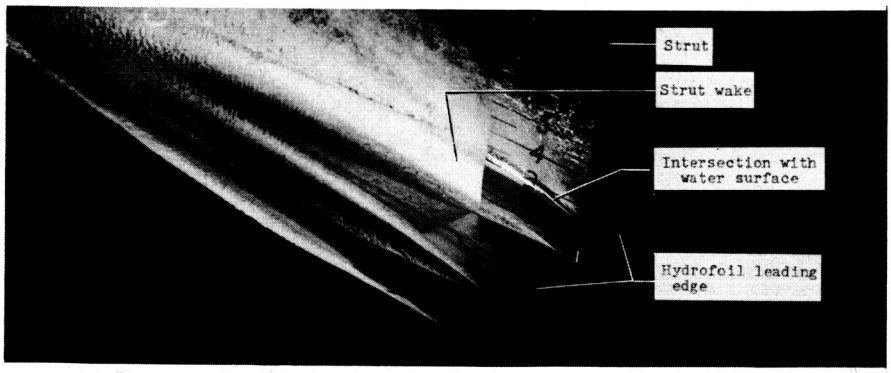

(b) $\alpha = 1.5^{\circ}$; V = 144.75 fps.

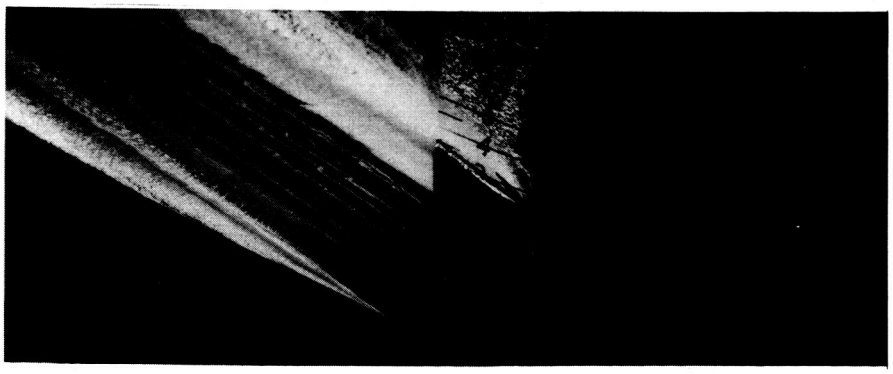

(c) $\alpha = 3.0^{\circ}$; V = 147.12 fps. L-60-8325

Figure 8.- Photographs of the flow about the aspect-ratio-3 cambered parabolic hydrofoil at three angles of attack.

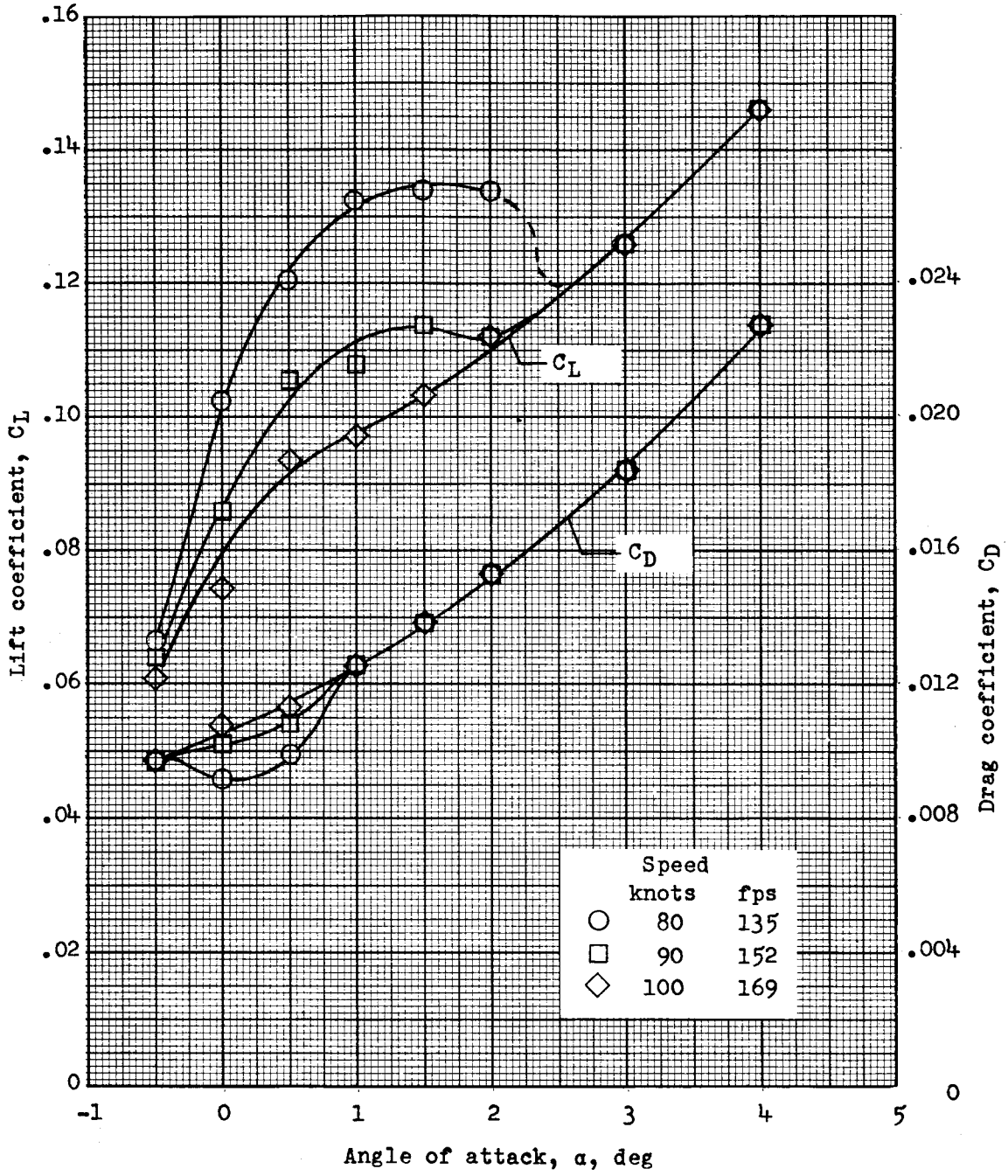

(a) Variation of lift and drag coefficients with angle of attack.

Figure 9.- Hydrodynamic characteristics of the aspect-ratio-3 cambered hydrofoil at constant speeds of 80, 90, and 100 knots. d/c = 0.5.

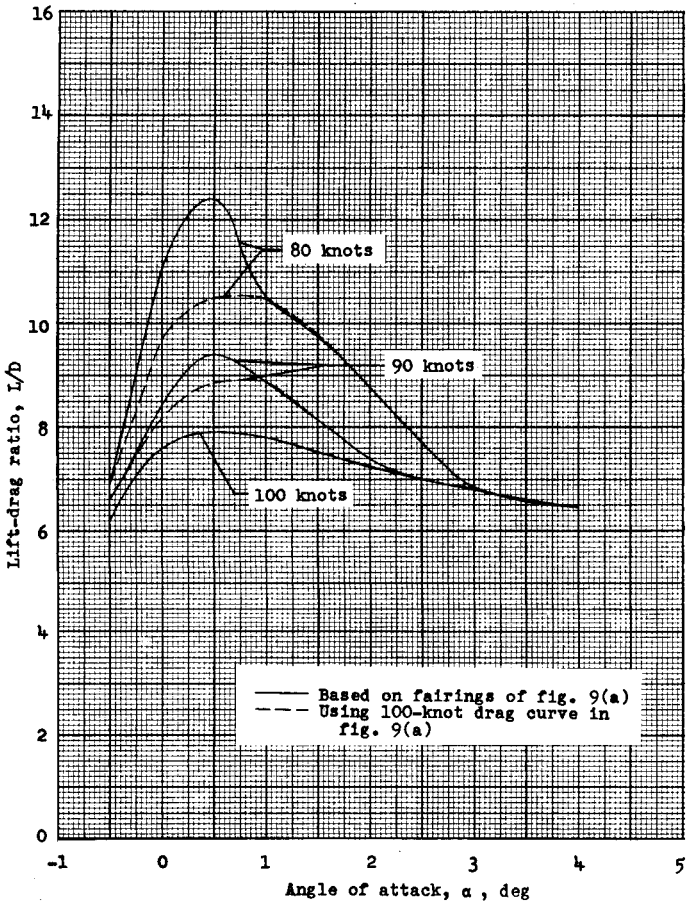

(b) Variation of lift-drag ratio with angle of attack.

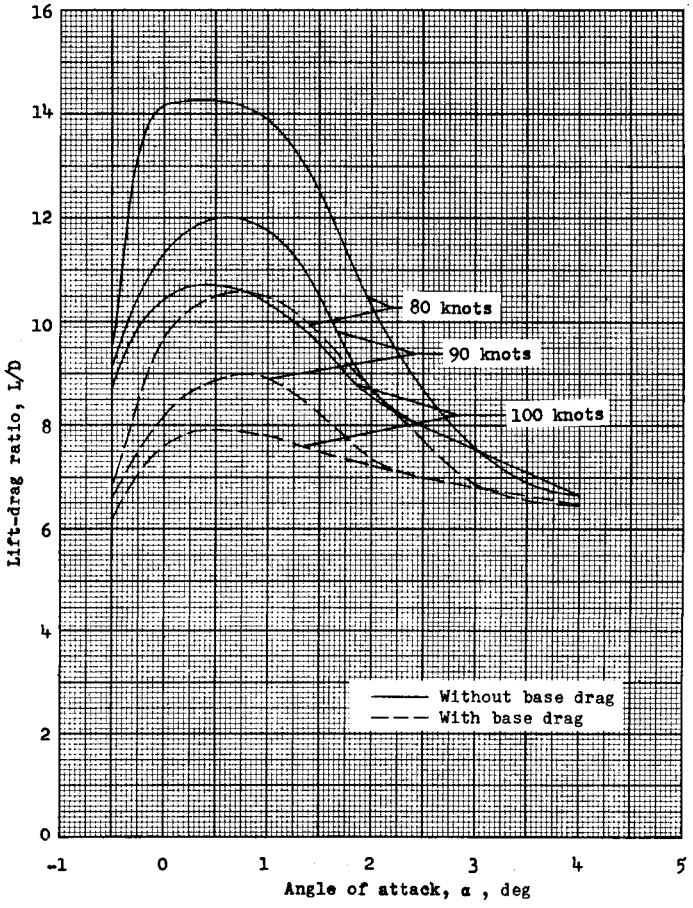

(c) Effect of hydrofoil base drag on lift-drag ratio.

Figure 9.- Concluded.

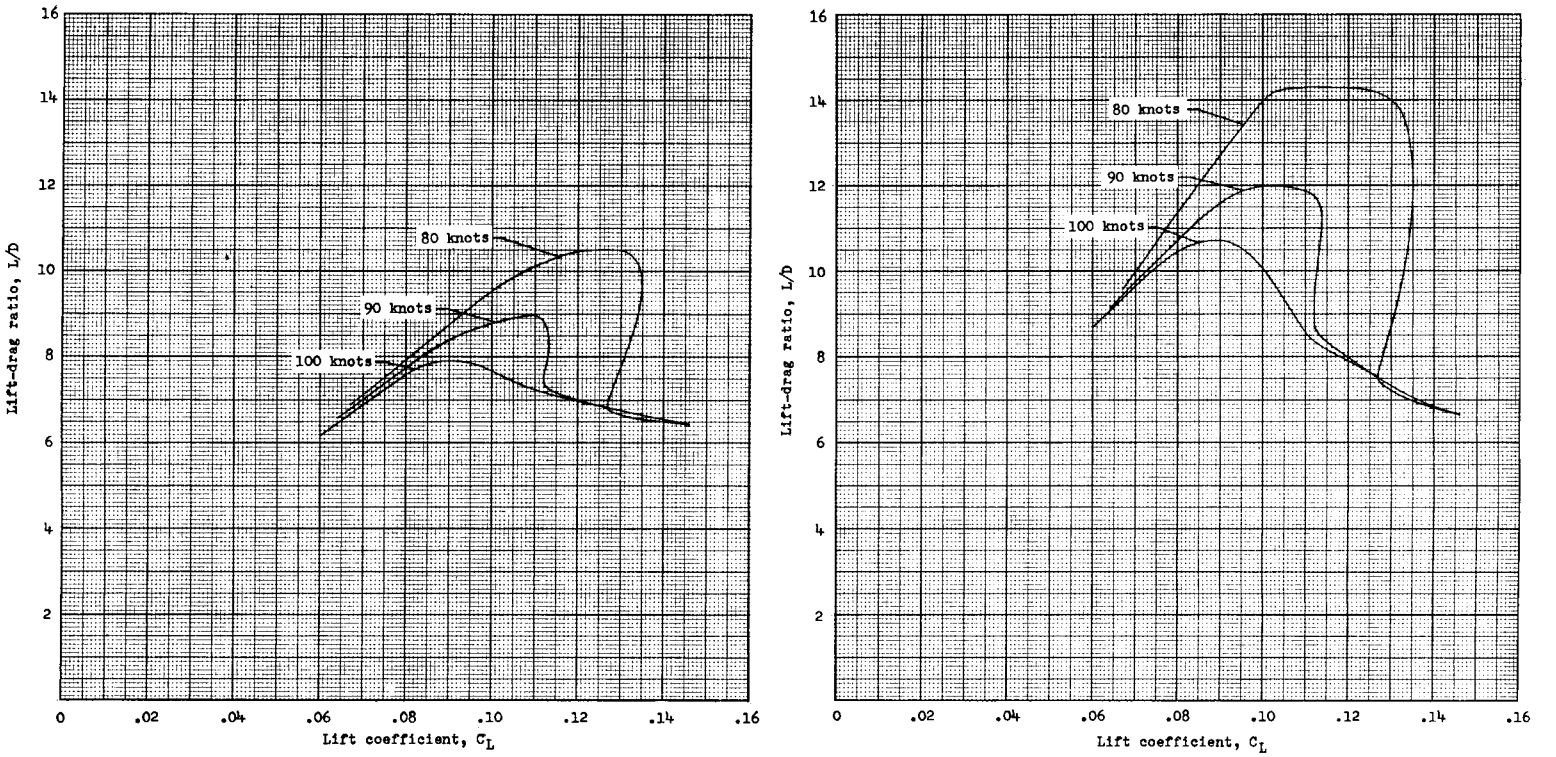

(a) Hydrofoil base drag included in drag.

(b) Hydrofoil base drag removed.

Figure 10.- Variation of lift-drag ratio with lift coefficient with and without base drag of hydrofoil.

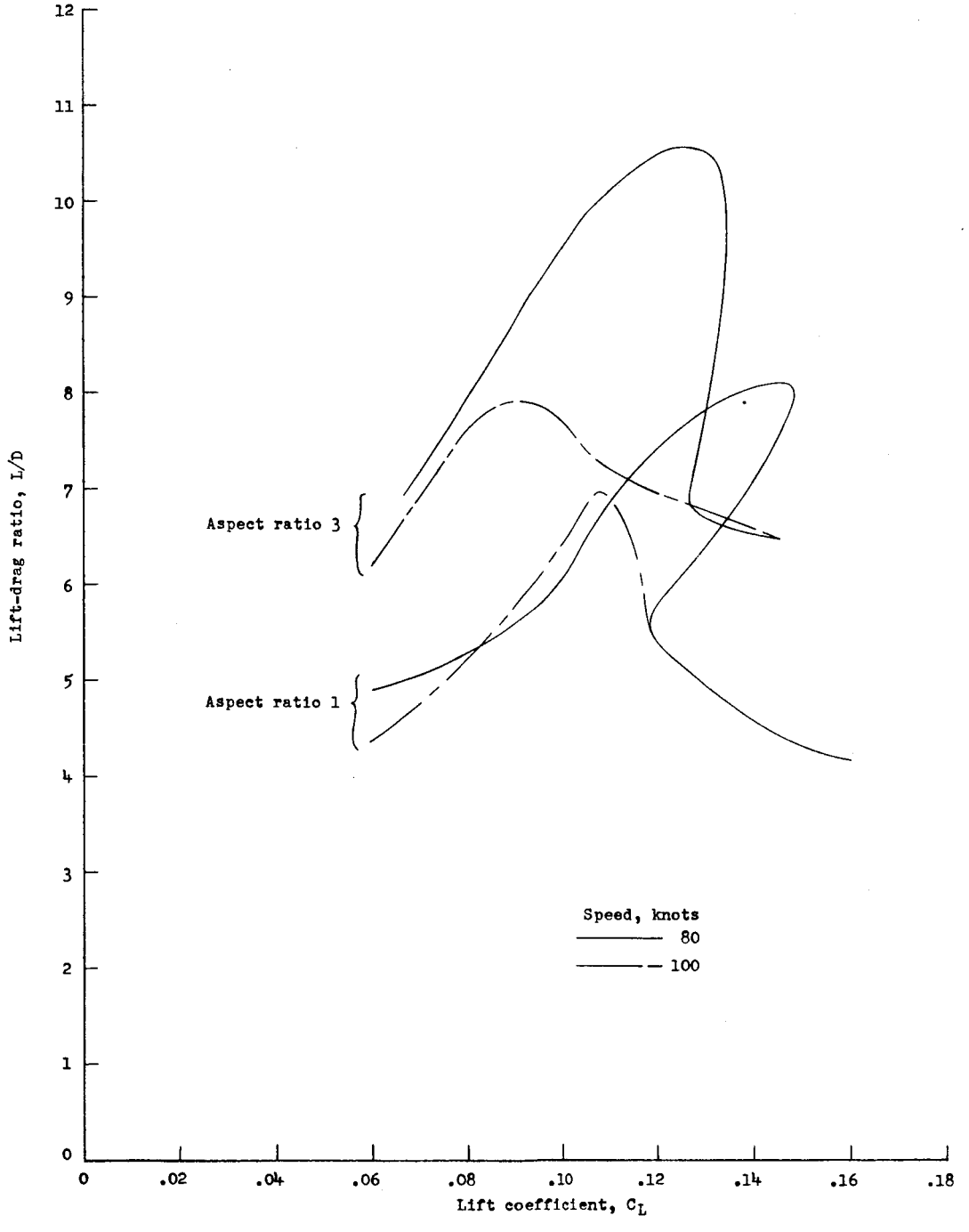

Figure 11.- Comparison of lift-drag ratios of aspect-ratio-3 cambered parabolic hydrofoil with the lift-drag ratios of the aspect-ratio-1 cambered parabolic hydrofoil. d/c = 0.5.